JOURNAL OF CATALYSIS **169,** 203–211 (1997)
ARTICLE NO. CA971673

Oxidative Dehydrogenation of Ethane and *n*-Butane on VO_x/Al_2O_3 Catalysts

T. Blasco,* A. Galli,*,[1] J. M. López Nieto,*,[2] and F. Trifiró†

*Instituto Tecnología Química, UPV-CSIC, Avenida Los Naranjos s/n, 46071 Valencia, Spain; and †Department of Industrial Chemistry and Materials, University of Bologna, V.le Risorgimento 4, 46031 Bologna, Italy

Received June 11, 1996; revised January 27, 1997; accepted February 24, 1997

γ-Al_2O_3-supported vanadium oxide catalysts (0–6.3 wt% V atoms) were prepared, characterized, and tested for the oxidative dehydrogenation (ODH) of both ethane and *n*-butane. The vanadium loading strongly influences the catalytic behavior of γ-Al_2O_3-supported vanadium oxide catalysts during the ODH of *n*-butane and ethane. While the catalytic activity in the ODH reactions increases with the vanadium loading, the selectivity to the corresponding olefins shows a maximum for catalysts with 3–4 wt% V atoms. In addition, the selectivity to oxydehydrogenation products during the ODH of butane was lower than the selectivity to ethene during the ODH of ethane. Associated VO_4 tetrahedra were observed by ^{51}V-NMR on catalysts with V loading lower than 5 wt%, while VO_6 octahedra were predominant on catalysts with higher V loading. In this way, although catalysts with octahedral V^{5+} species show higher catalytic activity, higher selectivity to oxydehydrogenation reactions was achieved on catalysts in which mainly tetrahedral V^{5+} species were observed. The number and nature of the acid sites also change with the vanadium loading. Thus, Lewis acid sites were observed mainly on catalysts with low V loading, while both Lewis and Brønsted acid sites were observed on catalysts with high V loading. Although V^{5+} species were observed mainly on calcined samples, V^{4+} species are observed on tested catalysts and their concentration depends on the alkane conversions used in the catalytic tests.

INTRODUCTION

Catalysts based on supported vanadium oxides are well known for the selective oxidation of hydrocarbons, but their catalytic properties depend on the metal oxide support and on the vanadium content (1–5). On Al_2O_3-supported vanadia catalysts, olefins and aromatic hydrocarbons are selectively transformed into oxygenated products on catalysts with vanadium content higher than the theoretical monolayer; however, for the oxidative dehydrogenation of alkanes, the best selectivities to the corresponding olefins are achieved only on catalysts with low vanadium loading (6–9). Furthermore, the selectivity to oxydehydrogenation products depends on the alkane fed and decreases in the order ethane > propane > *n*-butane (9–11).

Vanadia catalysts supported on Al_2O_3 have been characterized by a variety of physicochemical methods. The data obtained from Raman (12–16), ^{51}V NMR (15–17), ESR (18–20), XPS (14, 21), UV–Vis reflectance (19), EXAFS–XANES (22, 23), temperature-programmed reduction (12, 14, 23, 24), and infrared and microcalorimetric studies of adsorbed probe molecules (25–27) indicate that the type of vanadium species depends on the vanadium content. If a vanadium oxide monolayer completely covering the surface of the support should need 4.98×10^{14} molecules V_2O_5 cm^{-2}, the appearance of V_2O_5 crystallites on Al_2O_3 occurs at a vanadium loading of about 60% of the theoretical monolayer (14). At lower vanadium loadings, isolated and/or associated tetrahedral and/or octahedral V^{5+} species have been observed.

This paper reports the influence of the vanadium loading of alumina-supported vanadium oxide catalysts, under submonolayer coverages, on their catalytic properties for the oxidative dehydrogenation of ethane and *n*-butane using low alkane/oxygen ratios. The catalyst characterization was performed with the aim of elucidating the nature of the active and the selective sites for the oxydehydrogenation reactions.

EXPERIMENTAL

Catalyst Preparation

A series of alumina-supported vanadia catalysts were prepared by "wet" impregnation of a Girdler T126 γ-Al_2O_3 support ($S_{BET} = 188$ m^2 g^{-1}), ground and sieved to 0.042–0.059 cm, with an ammonium metavanadate solution (pH = 7). The concentrations of the solutions were selected to achieve vanadium loadings ranging between 0 and 8 wt% vanadium atoms. In addition, two catalysts were prepared by percolating a 0.05 *M* ammonium metavanadate solution through γ-Al_2O_3 support (400 ml of solution for 5 g of the

[1] On leave from the Department of Industrial Chemistry and Materials, University of Bologna, V.le Risorgimento 4, 46031 Bologna, Italy.
[2] To whom correspondence should be addressed.

0021-9517/97 $25.00

TABLE 1

Physicochemical Characteristics of Alumina-Supported Vanadium Oxide Catalysts

Sample	S_{BET} ($m^2\ g^{-1}$)	V content (wt%)[a]	V_2O_5 (10^{18} molecules m^{-2})	Coverage[b]	Lewis acid sites[c]	V^{4+} content[d]	H_2-TPR results[e]		
							T_M (°C)	H_2-uptake	AOS
A0	145	0	0.00	0	39.1	0	—	—	—
A1	150	1.5	0.61	0.12	25.9	v.l.i	503	2.54	3.3
A2	146	2.4	0.97	0.20	n.s.	v.l.i	488	4.13	3.3
A3	144	3.3	1.35	0.27	n.s.	n.s.			
A6	137	6.3	2.57	0.52	19.9	0.5	465	11.49	3.1
B4	137	4.3	1.77	0.36	30.1	0.4	475	5.06	3.8
B5	134	5.4	2.20	0.44	22.9	1.0	471	8.92	3.3

[a] Vanadium content, in wt% of V atoms, was determined by atomic absorption spectrometry.

[b] Considering 4.98×10^{18} molecules $V_2O_5\ m^{-2}$ as the amount of vanadium oxide necessary to obtain a monolayer (14), and the initial surface area of the support ($145\ m^2\ g^{-1}$).

[c] Determined from the intensity of the band at 1450 cm^{-1} in the IR spectra of pyridine desorbed at 150°C. n.s., not studied.

[d] V^{4+} content (a.u.) in calcined catalysts, determined from ESR. v.l.i, very low intensity of the ESR signal.

[e] Temperature of the maximum hydrogen consumption (T_M), H_2 consumption in mol H_2/g of catalyst, and the corresponding average oxidation state after reduction (AOS).

support). The solutions were adjusted with nitric acid to achieve final pH values of 7 (sample B4) and 3 (sample B5).

The catalysts were finally calcined at 600°C during 6 h. The characteristics of the catalysts are listed in Table 1. The vanadium coverages indicated in Table 1 were calculated considering that 4.98×10^{18} molecules $V_2O_5\ m^{-2}$ is the vanadium loading necessary to obtain a monolayer of vanadium oxide completely covering the surface of the support (14).

Catalytic Test

The catalytic tests for the oxidative dehydrogenation (ODH) of ethane were carried out in a fixed-bed quartz tubular reactor (16-mm i.d., 500-mm length) equipped with a coaxial thermocouple for temperatures profiles. Catalyst samples 0.3 to 1.3 g and particle sizes between 0.25 and 0.42 mm were mixed with variable amounts of SiC (0.59 mm particle size) to keep a constant volume in the catalyst bed (3 cm^3). The reaction was studied in the temperature interval 450–600°C using an ethane/oxygen/helium molar ratio of 4/8/88. The total flow was varied from 100 to 200 ml min^{-1} obtaining different contact times [$W/F = 15$ to 80 g_{cat} h $(mol\text{-}C_2)^{-1}$]. Analysis of reactants and products was carried out by gas chromatography, using two column types: (i) Porapak Q (3.0 m × 1/8 in.); (ii) molecular sieve 5A (1.5 × 1/8 in.). Analysis of C_4 hydrocarbons was carried out by gas chromatography, using a 23% SP-1700 Chromosorb PAW (30 × 1/8 in.) column (11).

Blank runs in the temperature interval 450–600°C were carried out substituting the catalyst by SiC, at the lowest total flow used in the present study (100 ml min^{-1}). Under our reaction conditions the presence of homogeneous reaction can be neglected.

Catalyst Characterization

The BET surface area of the samples, S_{BET}, was obtained in an ASAP 2000 apparatus, following the BET method from N_2 adsorption isotherms at 77 K and taking a value of 0.164 nm^2 for the cross section of N_2.

Diffuse reflectance (DR) spectra in the UV–visible region were collected with a Shimazdu UV-2010 PC spectrophotometer equipped with a reflectance attachment.

Solid-state ^{51}V NMR spectra were measured at ambient temperature on a Varian VXR-400S WB spectrometer at 105. 1 MHz, using a high-speed MAS Doty probe with zirconia rotors (5 mm in diameter). The spectra were recorded with pulses of 1 μs corresponding to a flip angle of $\pi/18$ rad, to avoid signal distortions of the $I = 7/2$ nuclei. The ^{51}V chemical shifts are referred against liquid $VOCl_3$, using $Mg_3(VO_4)_2$, whose chemical shift is −554 ppm, as secondary reference.

The ESR spectra were recorded at room temperature on a Varian E-109 spectrometer working at 9.3 GHz (X-band) with 100-kHz field modulation. DPPH ($g = 2.0036$) was used as standard to measure the g values.

Infrared spectra of adsorbed pyridine were obtained with a Nicolet 710 FTIR spectrophotometer. Wafers of 10 mg cm^{-2} were mounted in a Pyrex vacuum cell fitted with CaF_2 windows. The samples were degassed at 400°C for 2 h and cooled at room temperature (RT) to obtain the original IR spectra. Then, pyridine was admitted at room temperature and degassed for 1 h to remove the physisorbed fraction, and the spectra were taken at room temperature. Finally, pyridine was desorbed at 150 and 250°C.

Temperature-programmed reduction (TPR) results were obtained with a Micromeritics apparatus. Samples of 100 mg were first treated in argon at room temperature

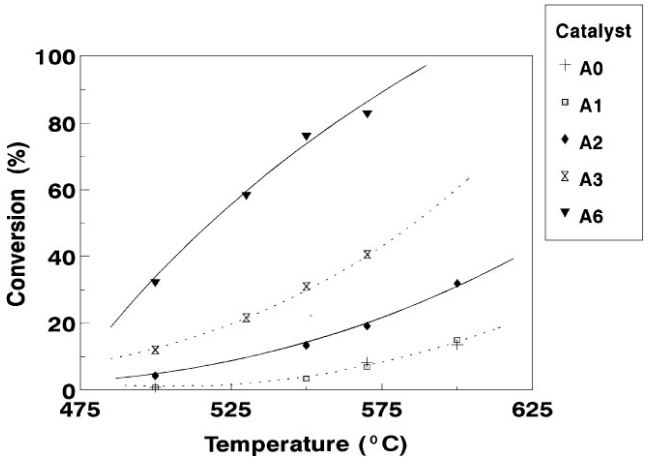

FIG. 1. Variation of the conversion of ethane with reaction temperature on supported vanadium oxide catalysts. Experimental conditions: $W = 0.5$ g; total flow = 200 ml min^{-1}.

for 1 h. The samples were subsequently contacted with an H_2/Ar mixture (H_2/Ar molar ratio of 0.15 and total flow of 50 ml min^{-1}) and heated, at a rate of 10°C min^{-1}, to a final temperature of 1000°C.

RESULTS

Catalytic Results

Variation of the ethane conversion with the reaction temperature on Al_2O_3-supported vanadium oxide catalysts is shown in Fig. 1. It can be seen that ethane conversion increases with reaction temperature and vanadium loading. In fact, the rate of ethane conversion per gram of vanadium increases with vanadium loading (Fig. 2).

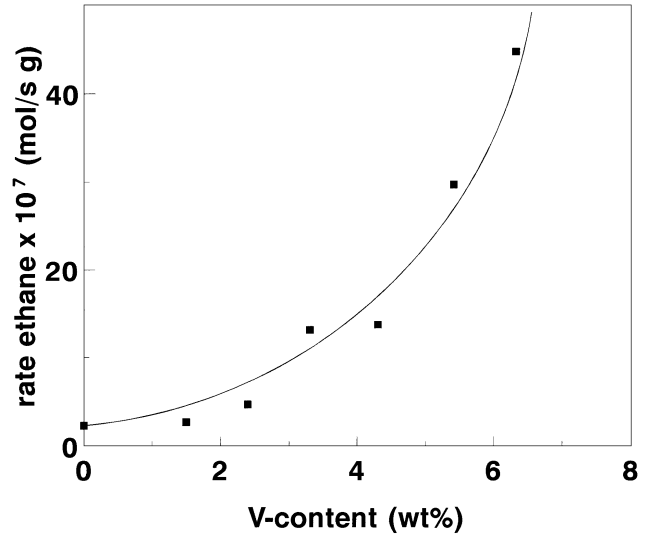

FIG. 2. Variation of the rate of ethane conversion with catalyst vanadium loading. Reaction temperature = 500°C.

TABLE 2

Oxidative Dehydrogenation of Ethane on Al_2O_3-Supported Vanadium Oxide Catalysts[a]

Sample	V content (wt%)	Conversion (%)	Yield (%)			Selectivity to C_2H_4 (%)
			CO	CO_2	C_2H_4	
A0	0	8.0	3.1	4.3	0.5	8.1
A1	1.5	6.7	1.2	1.0	4.5	67.6
A2	2.4	18.8	6.8	2.3	9.7	51.5
A3	3.3	40.2	16.3	2.8	21.1	52.5
B4	4.3	42.0	18.4	3.1	20.5	48.9
B5	5.4	58.0	33.6	4.6	19.7	34.0
A6	6.3	82.2	58.3	10.5	13.4	16.3

[a] Experimental conditions: $W = 0.5$ g; total flow = 200 ml min^{-1}; temperature = 570°C.

Table 2 summarizes the catalytic properties of Al_2O_3-supported vanadium oxide catalysts during the oxidative dehydrogenation of ethane at 570°C. In all cases, ethene and carbon oxides (CO and CO_2) were the only reaction products obtained. Although ethane conversion increases with catalyst vanadium content, the highest yield of ethane was obtained on catalysts with 3 to 5 wt% V atoms. Thus, the incorporation of vanadium initially increases the yield to ethene, obtaining catalysts with high selectivity to this product; however, although the activity of ethane conversion increases, the selectivity to ethene decreases with vanadium loadings beyond 4 wt%.

The variation of the selectivities to the main reaction products with vanadium loading at 570°C and an ethane conversion of 20% is shown in Fig. 3. The selectivity to

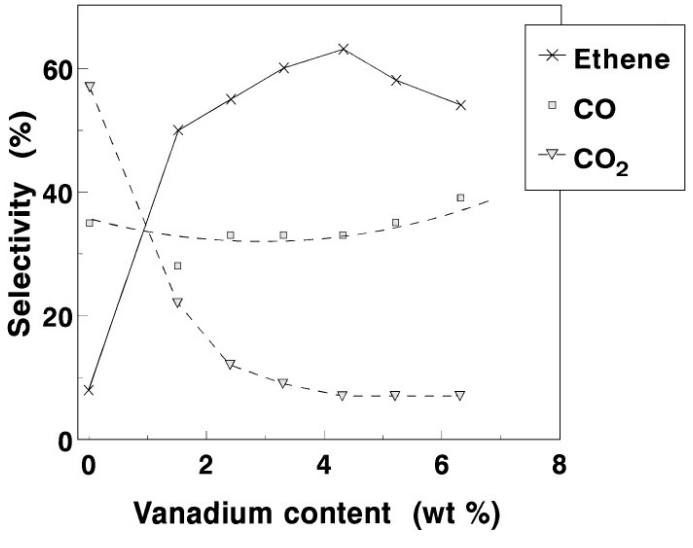

FIG. 3. Variation of the selectivities to ethene, CO, and CO_2 with vanadium loading. Reaction temperature = 570°C; ethane conversion = 20%.

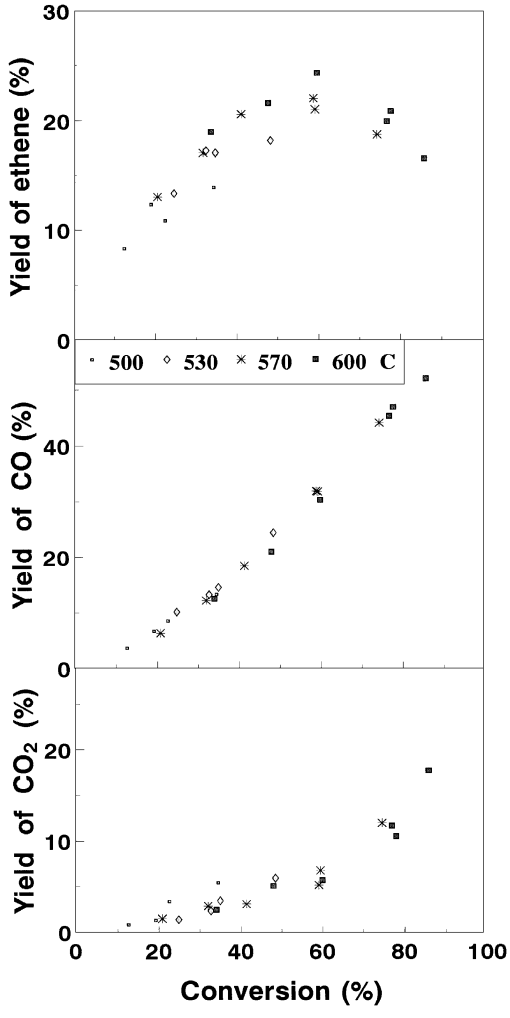

FIG. 4. Variation of the yields of ethene, CO, and CO_2 with ethane conversion on catalyst B4 at different reaction temperatures.

ethene shows a maximum on catalysts with a vanadium content of 3–5 wt%, whereas selectivity to CO_2 decreases and selectivity to CO increases with vanadium content. Thus, the incorporation of vanadium increases the formation of ethene, but, at high vanadium loadings, the consecutive reactions also increase.

Figure 4 shows the variation of the yields of the main reaction products with ethane conversion on sample B4 at different temperatures. At all reaction temperatures studied, the yield of ethene initially increases with ethane conversion (Fig. 4a), reaching a maximum for conversions of 30–40%. In addition, it can also be seen that the yield of ethene (and the selectivity to ethene) increases with reaction temperature.

On the other hand, and according to the results shown in Fig. 4, it can be concluded that ethene is a primary and unstable product, whereas CO and CO_2 can be considered primary and secondary products.

Table 3 shows the catalytic behavior of samples B4 and B5 during the ODH of *n*-butane. Strong differences between the catalysts are observed. In addition, it can be observed that the yield of butenes obtained on B5 catalysts is lower than on pure alumina. Since B4 and B5 catalysts present similar catalytic behavior during the ODH of ethane, it can be concluded that the V loading of alumina-supported catalysts influences more strongly their catalytic properties during the ODH of *n*-butane. We may note that, independently of vanadium loading, the selectivity to oxydehydrogenation products achieved during the ODH of *n*-butane was lower than during the ODH of ethane.

Catalyst Characterization

Figure 5 shows the UV–Vis spectra of calcined (Fig. 5a) and tested samples (Fig. 5b). The absorption band at 280–290 nm indicates the presence of tetrahedral V^{5+} species (8, 9, 19). In addition to this, bands at 350–400 nm (on calcined samples with high vanadium loading) and 550–1400 nm (on tested samples) are also observed. The first ones are related to octahedral V^{5+} species, and the second ones to V^{4+} species (8, 9, 19).

Figure 6 shows the ^{51}V wide-line (wl) and magic-angle-spinning (MAS) spectra of samples B4 and A6. The valley between the peaks in the nonspinning spectra is produced by the preacquisition delay of the spectrometer. The spectra recorded under MAS are characterized by intense spinning sideband patterns. The use of different spinning rates allowed us to determine the main line position.

^{51}V NMR has been shown to be a powerful technique in the characterization of the V^{5+} environment in supported vanadium oxide catalysts (15–17). Comparison of the NMR

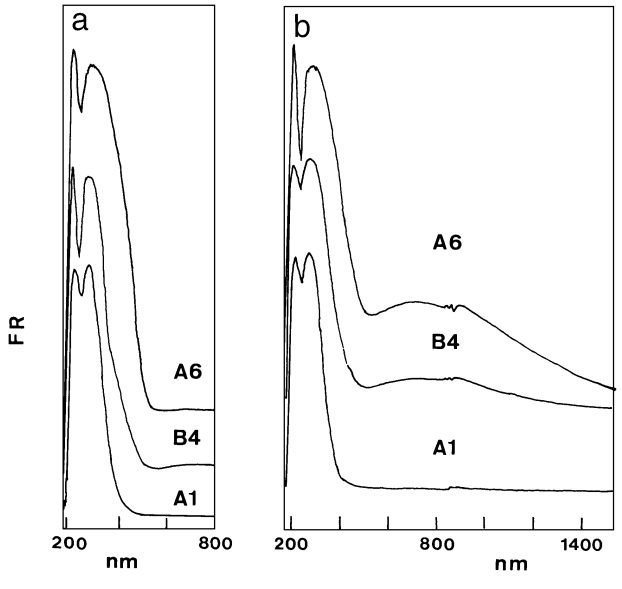

FIG. 5. Diffuse reflectance (UV–Vis) spectra of calcined (a) and tested (b) samples.

TABLE 3

Oxidative Dehydrogenation of *n*-Butane on Al_2O_3-Supported Vanadium Oxide Catalysts[a]

Sample	T (°C)	X_T (%)[c]	Y_{ODH} (%)[d]	Selectivity (%)					
				1-C_4H_8	*trans*-2-C_4H_8	*cis*-2-C_4H_8	C_4H_6	CO	CO_2
A0	400	2.16	0.67	7.65	9.60	4.99	8.84	13.2	48.0
	450	6.2	1.6	5.93	5.95	4.90	9.64	16.7	52.5
	500	13.4	3.1	5.98	5.62	4.92	7.83	17.5	52.2
B4	400	7.01	2.9	9.2	13.9	10.4	8.2	20.8	35.5
	450	20.1	4.5	5.25	6.46	5.18	5.71	33.8	42.4
	500	43.0	4.4	2.43	2.61	2.04	3.15	45.0	43.8
B5	400	11.9	1.0	1.37	3.06	2.27	1.71	40.4	49.8
	450	30.6	1.1	0.86	1.14	0.88	0.87	48.6	46.9
	500[b]	39.2	1.4	0.88	0.93	0.81	0.84	54.1	41.6

[a] $W/F = 8.0$ g_{cat} h (mol-C_4)$^{-1}$, and a *n*-butane/oxygen/helium molar ratio of 5/20/75 (Ref. 11).
[b] $W/F = 2.7$ g_{cat} h (mol-C_4)$^{-1}$.
[c] *n*-Butane conversion.
[d] Yield of oxydehydrogenation products (1-butene, *cis*-2-butene, *trans*-2-butene, and butadiene).

spectra of the catalysts with reference compounds provides information about the coordination symmetry and, for tetrahedral coordination, the number of bridging V–O–V oxygen atoms (*n* in the $Q^{(n)}$ notation) (15).

The wide-line spectrum of sample B4 (Fig. 6a) exhibits three features at ca. −300, −544, and −900 ppm, and the center band in the MAS spectrum appears at $\delta = -580$ ppm. In agreement with previous publications the wide-line spectrum can be interpreted as the contribution of two different signals (11, 15–17, 24). The low-field peak in the static spectra of Fig. 6 indicates the presence of vanadium in octahedral coordination; however, due to distortion of the spectrum we cannot establish the symmetry of this octahedral site. The second signal, characterized by a maximum between −500 and −600 ppm (at ca. −544 ppm), dominates the wide-line spectrum and appears at ca. −580 ppm under spinning. Comparison with model compounds allowed us to attribute this signal to the presence of polymeric tetrahedral V^{5+} as in metavanadates (15–17). We must indicate that we were not able to identify the peak corresponding to the octahedral V^{5+} species in the MAS spectrum, probably because of the presence of numerous spinning side bands of the predominant signal of tetrahedral V^{5+} species.

Different ^{51}V NMR spectra are obtained for sample A6 (Fig. 6b). The wide-line spectrum of this sample is characteristic of an almost axially symmetric chemical shift tensor

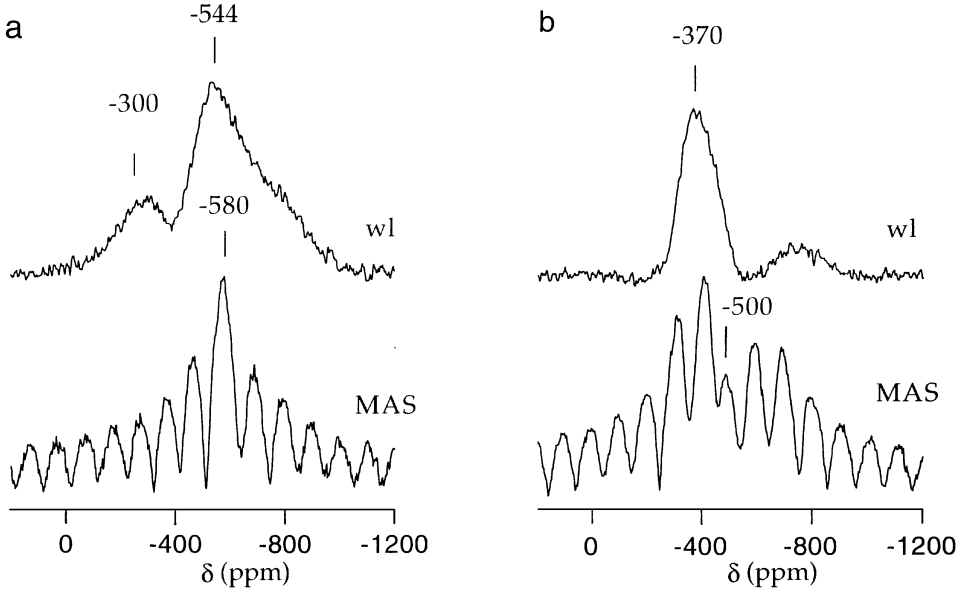

FIG. 6. ^{51}V wide-line (wl) and MAS-NMR spectra (spinning rate of 9 kHz) of VO_x/Al_2O_3 catalysts: B4 (a) and A6 (b).

with an intense peak at −370 ppm and a second component at around −900 ppm. The MAS center band appears at −500 ppm (Fig. 6b). The spectroscopic parameters of this signal as well as the spinning side band pattern are very similar to those of "type a" signal reported by Eckert and Wachs (15) for V^{5+} in distorted octahedral geometry, as in ZnV_2O_6 or PbV_2O_6, and different from those of V_2O_5.

Thus, the ^{51}V NMR results indicate that crystalline V_2O_5 has not been formed even in sample A6 with the highest V coverage studied here. In this sample, V^{5+} is mostly in a distorted octahedral environment, whereas in sample B4, with lower V coverage, mainly polymeric tetrahedral species are present. This is in good agreement with previous publications (15–17, 24) showing that polymeric tetrahedral vanadium is favored at low coverages, while the concentration of octahedral V^{5+} species increases with surface vanadium concentration.

Figure 7 shows the ESR spectrum of sample B5 after the catalytic test in the ODH of ethane. A similar spectrum was observed before the catalytic test, although with a lower intensity. This spectrum can be assigned to V^{4+} ($3d^1$) in an axially symmetric environment. The hyperfine structure is due to the interaction of the unpaired electron with the nuclear magnetic moment of vanadium with $I = 7/2$ (natural abundance 99.76%), giving rise to eight parallel and eight perpendicular components. The resolution of the hyperfine structure in the spectra indicates the presence of highly dispersed V^{4+} ions. The g values and the hyperfine coupling constants of the V^{4+} signal are $g_\parallel = 1.947$ (±0.005) $g_\perp = 1.965$ (±0.005), $A_\parallel = 190$ (±3 G), and $A_\perp = 78$ G (±3 G). Similar spectra, without any additional signal, were also recorded at 77 K.

Well-resolved signals with different ESR parameters have been previously obtained for Al_2O_3-supported vanadium oxide catalysts, which in some cases have been reported to depend on the vanadium content and reduction pretreatment (8, 18–20). Eon *et al.* (8) recorded the ESR spectra of some VO_x/Al_2O_3 catalysts after the ODH of propane and obtained a signal with spectral parameters ($g_\perp = 1.982$, $g_\parallel = 1.919$, $A_\perp = 70$ G, and $A_\parallel = 190$ G) different from those obtained in the present work, which was attributed to an amorphous surface vanadium oxide phase. In most of these publications (8, 18–20) the ESR signals are assigned to $(V{=}O)^{2+}$ in a tetragonally distorted octahedral environment with C_{4v} symmetry. The degree of the tetragonal distortion, and thus the strengh of the V=O bond, is estimated by the parameter $B = \Delta g_\parallel / \Delta g_\perp (\Delta g_\parallel = g_\parallel - g_e, \Delta g_\perp = g_\perp - g_e)$ that, in the limit of undistorted octahedral symmetry, takes a value of 1. In our case, $B = 1.5$, which is within the range 1.1–4.5 reported by other authors (20) and is relatively low, suggesting that we are dealing with $(V\cdots O)$ species rather than with V=O. The assignment of the ESR signals to octahedral V^{4+} is usually supported on the detection of the signal at room temperature, since, in general, it is admitted that tetrahedral V^{4+} is observable only at low temperature due to relaxation effects. In a recent publication on the characterization of alumina-supported vanadium catalysts (18), however, a signal

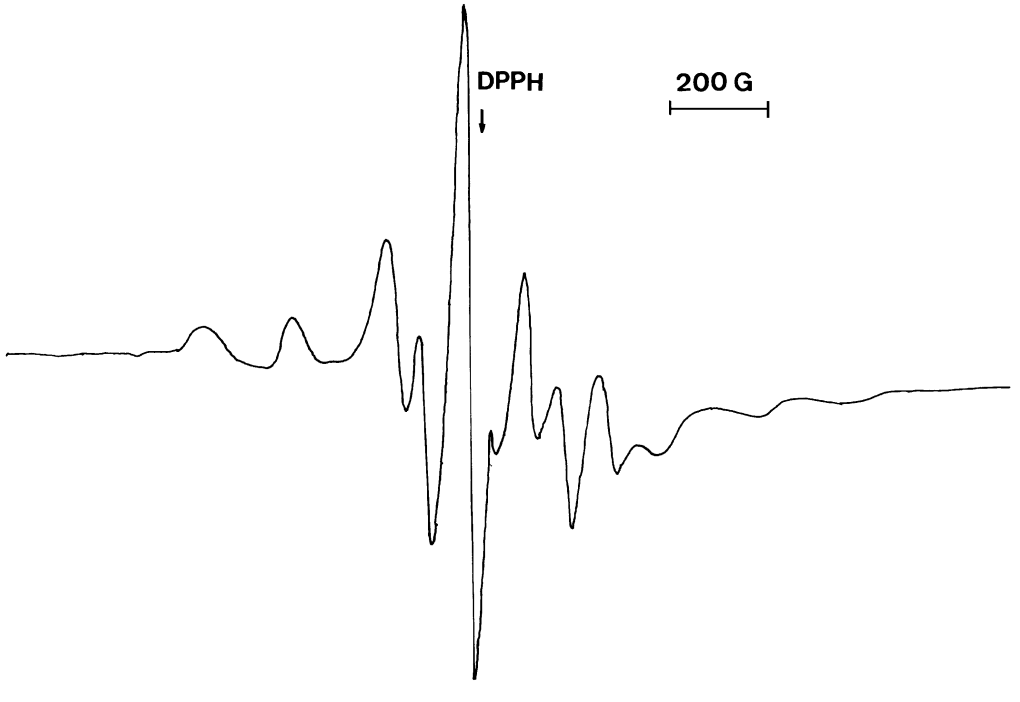

FIG. 7. ESR spectra of samples B5 after the catalytic test.

detectable at 293 K and characterized by $g_\perp = 1.979$–1.985, $g_\parallel = 1.931$–1.934 (depending on the sample), $A_\perp = 74$ G, $A_\parallel = 200$ G has been assigned to V^{4+} in a distorted tetrahedral environment. Thus, we can conclude that the ESR spectra shown in Fig. 7 can be tentatively attributed to V^{4+} in an octahedral coordination, although a more detailed study would be required to better establish the coordination environment of the V^{4+} in these catalysts.

Similar spectra with a different intensity were obtained for all the catalysts studied here. Table 1 shows the relative concentrations of V^{4+} species in the calcined catalysts, determined from the intensity of the ESR spectra. For catalysts of series A, the intensity of the V^{4+} ESR signal slightly increases with vanadium loading. Comparison of these samples with B4 and B5 catalysts, prepared by a different method, shows the presence of a relatively high concentration of V^{4+} atoms in sample B5 (prepared at pH = 3). This result suggests that the catalyst preparation procedure influences the oxidation state of the incorporated V atoms in the calcined catalysts.

On the other hand, we also monitored by ESR the relative concentration of V^{4+} species on catalyst B4 with the ethane conversion level achieved (Fig. 8). It can be seen that the relative amount of V^{4+} species increases with ethane conversion. Similar behavior is observed for all the catalysts studied here, although the ESR spectrum of sample A6 after reaction shows, superimposed to the hyperfine structure, a broad and unstructured line produced by the dipolar interactions, indicating the presence of associated V^{4+}. This can be due to the higher degree of reduction of this sample provoked by its higher activity in the ODH reaction of ethane.

Pyridine adsorption was followed by infrared spectroscopy to identify the number and nature of acid sites in alumina-supported catalysts. Figure 9 shows the FTIR spectra of the catalysts after pyridine adsorption

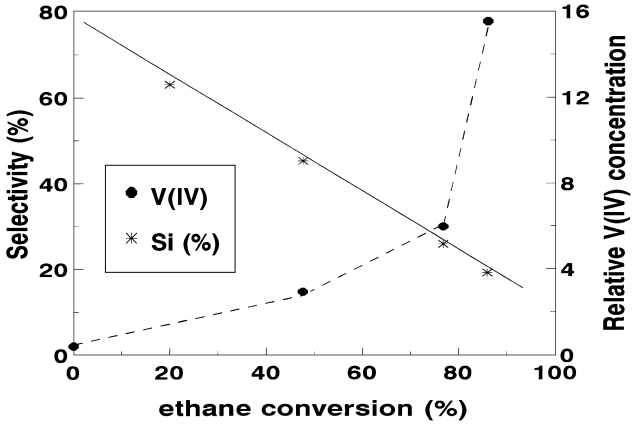

FIG. 8. Variation with ethane conversion (at 600°C) of the selectivity to ethene and the amount of V^{4+} species of the corresponding tested B4 sample.

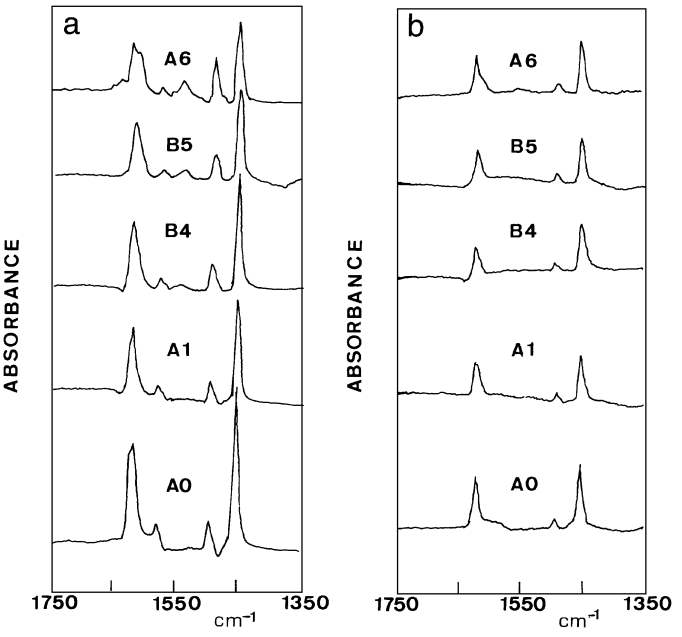

FIG. 9. FTIR spectra of pyridine adsorbed on VO_x/Al_2O_3 catalysts after evacuation at 150°C (a) and 250°C (b).

and subsequent evacuation at 150°C (Fig. 9a) and 250°C (Fig. 9b).

After evacuation at 150°C, Lewis acid sites (bands at 1450 and 1578 cm^{-1}) could be observed on both support and catalysts, whereas Brønsted acid sites (band at 1540 cm^{-1}) were observed only on samples with vanadium content higher than 4 wt% (Fig. 9a). For these latter samples, a vibration band at 1638 cm^{-1}, which can also be related to Brønsted acid sites, is observed (25). Additional bands at 1492 and 1615 cm^{-1}, associated with the presence of pyridine, were also observed in all the catalysts. However, their assignment to specific type of acid sites is not clear. Comparison of the spectra in Fig. 9a indicates that the higher the catalyst vanadium content, the lower the number of Lewis acid sites (Table 1).

After evacuation at high temperatures only Lewis acid sites are observed (Fig. 9b). Under these conditions, the intensity of the characteristic band at 1450 cm^{-1} decreases for all the samples presenting similar intensities for the support and the catalysts. Thus, for the alumina-supported vanadia catalysts studied here, the total number of Lewis acid sites decreases, while the number of Brønsted acid sites increases with vanadium loading. According to this, and in agreement with previous results (25), it can be concluded that Lewis acid sites are due to γ-Al_2O_3, whereas Brønsted acid sites are related to vanadium oxide incorporation.

Infrared spectra in the hydroxyl region of the support, evacuated at 400°C, show two absorption bands of free hydroxyl groups at 3750 and 3680 cm^{-1}. These bands are present only on pure alumina and catalysts with low vanadium loading, indicating that the free hydroxyl groups

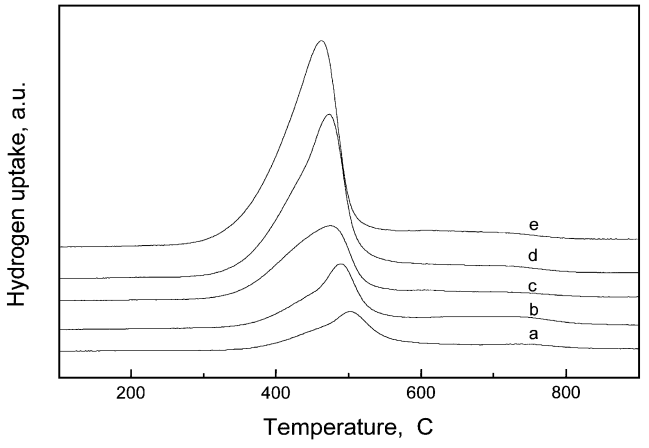

FIG. 10. TPR patterns of VO_x/Al_2O_3 catalysts. Samples: (a) A1, (b) A2, (c) B4, (d) B5, (e) A6.

disappear after the incorporation of larger amounts of vanadium.

TPR patterns of the studied catalysts are shown in Fig. 10. Three peaks can be observed: an intense peak at 463–505°C with a shoulder at 450°C and a broad peak at temperatures above 600°C. The TPR results summarized in Table 1 indicate that the temperature of maximum hydrogen consumption decreases and the amount of hydrogen consumption increases with vanadium loading. On the other hand, and considering a total V^{5+}-to-V^{3+} reduction, the average oxidation state (AOS) after H_2 reduction has been calculated and included in Table 1. It can be seen that, except in the case of sample B4 (with an AOS of 3.8), the catalysts present AOSs of 3.1–3.3.

These results are in agreement with those observed by other authors (14, 23, 24), although the temperature of maximum hydrogen consumption changes depending on the experimental conditions used. The amounts of H_2 consumption for the catalysts studied are higher than those observed by Koranne *et al.* (24) but similar to those reported by Haber *et al.* (23). The discrepancies between these two papers could be due to different amount of H_2 adsorbed, remaining on the catalyst surface as V−O−H (24). If we consider this H_2 adsorption, the real AOS of the catalyst tested will be near 4+, and the difference between the real and estimated AOSs will be related to the amount of H_2 adsorbed.

DISCUSSION

According to the results shown in Fig. 4, it can be concluded that ethene is a primary and unstable product, whereas CO and CO_2 are primary and secondary products. Thus, a network for the ODH of ethane is proposed in Scheme 1 in which CO and CO_2 are formed by the deep oxidation of both ethane and ethene.

On the other hand, from the catalytic and characterization results, three types of active sites can be proposed on VO_x/Al_2O_3 catalysts: (i) Vanadium-free alumina sites, the number of which decreases with increasing vanadium loading, are active but nonselective in the ODH of ethane. (ii) Polymeric tetrahedral V^{5+} species, which are formed mainly on catalysts with vanadium loading lower than 5 wt%, are active and selective in the formation of ethene. (iii) Polymeric VO_6 octahedra, observed mainly on catalysts with vanadium loading higher than 5 wt%, are active in the oxidation of ethane to ethene but also in the consecutive reaction of ethene to carbon oxides.

The highest selectivity to ethene in the ODH of ethane is obtained on catalysts in which tetrahedral vanadium species are predominant; however, although this also occurs for the ODH of *n*-butane, the selectivity to olefins was lower than in the oxidation of ethane. In previous works, it has been proposed that the selectivity to C_4-olefins can be related to the acid–base character of the catalyst, in the sense that the higher the acid character the lower the selectivity to C_4-olefins (9–11).

IR results of pyridine adsorption/desorption indicate that the catalysts present Lewis acid sites at low vanadium content and both Lewis and Brønsted acid sites at high vanadium loading, the latter showing the higher acid strength. Thus, Brønsted acid sites are related mainly to octahedral V^{5+} species; however, Lewis acid sites correspond mainly to the support and their number decreases when the V loading increases. In addition, since the octahedral vanadium species present generally low selectivity, the fact that these species show a higher acid character can contribute to the extremely low selectivity of these catalysts during the ODH of *n*-butane.

The importance of the acid character of both support and catalysts was also proposed to explain the catalytic properties of supported vanadium catalysts during the oxidation of methanol and heptanol (27). It was observed that the acid character of alumina influences the catalytic properties of vanadium-containing catalysts. Thus, alumina shows high selectivities to dimethyl ether or *n*-heptene during the

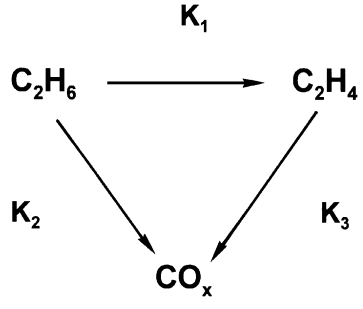

SCHEME 1. Network of the oxidative dehydrogenation of ethane on alumina-supported vanadium oxide catalysts.

oxidation of methanol or *n*-heptanol, respectively, and these selectivities increase with decreasing vanadium loading.

It is known that olefins are adsorbed on pure alumina at 300°C, forming alkenylcarbonium ions, to a degree that depends on the olefin, decreasing in the order 1-butene > propene > ethene (29). The lower selectivity to olefins in the oxidation of *n*-butane when compared with ethane can be attributed to the higher adsorption of *n*-butenes on the alumina support favoring a deep oxidation. Then, the contribution of the support to the catalytic properties of supported vanadium oxide catalysts must be considered.

On the other hand, although mainly V^{5+} species are observed on calcined samples, the number of V^{4+} species on the tested catalysts increased with the ethane conversion level (Fig. 8). The appearance of V^{4+} species has also been observed after the ODH of propane on alumina-supported vanadium oxide catalysts (8). However, the role of V^{4+} species is not clear. According to Ishida *et al.* (30), the reduction of Al_2O_3-supported vanadium oxide catalysts produces new Lewis acid sites associated with the reduced vanadium species formed. In our samples, an opposite trend between selectivity to ethene and the reduction degree of V species with the conversion of ethane is observed (Fig. 8). At high ethane conversion, the vanadium is partially reduced and can also favor a deep oxidation of both ethane and ethene decreasing the selectivity to ethene. The negative role of the presence of V^{4+} species could also contribute to the lower selectivities to olefins obtained during the ODH of *n*-butane, since in this case a higher degree of catalyst reduction can be expected.

The effect of V^{4+} on olefin selectivity proposed here seems to be inconsistent with previous publications on the oxidation of *n*-butane or *o*-xylene on V–P–O and VO_x/TiO_2 catalysts, respectively (31). For these systems, an effective V^{4+}/V^{5+} ratio near 1 is required to obtain the maximum selectivities to partially oxygenated products. Opposite to the ODH reactions, however, a negative effect of the presence of acid sites on the selectivity to partial oxygenated products is not observed, and thus, V^{4+} species can play a different role in O-insertion reactions than in the ODH of alkanes.

The results presented in this paper allows us to conclude that although both octahedral and tetrahedral V^{5+} species are active and selective in the ODH of ethane, the former show higher activity but lower selectivity, especially during the ODH of *n*-butane, due to the higher rate of consecutive reactions. This effect could be attributed to the higher acidity and reducibility of the VO_6 octahedra as can be deduced from the catalyst characterization results. In addition, the contribution of the vanadium-free support must be considered, especially during the ODH of *n*-butane.

ACKNOWLEDGMENTS

The authors acknowledge the financial contribution from the European Human Capital Mobility Project (CHRX-CT92-0065). T.B. and J.M.L.N. also acknowledge financial support from the Comisión Interministerial de Ciencia y Tecnología, CICYT, Spain (Project MAT 94-0898).

REFERENCES

1. Hucknall, D. J., *in* "Selective Oxidation of Hydrocarbons." Academic Press, New York, 1974.
2. Dadyburjor, D. B., Jewur, S. S., and Ruckenstein, E., *Catal. Rev. Sci. Eng.* **19**, 293 (1979).
3. Wainwright, M. S., and Foster, N. F., *Catal. Rev. Sci. Eng.* **19**, 211 (1979).
4. Bond, G. C., and Tahir, S. F., *Appl. Catal.* **71**, 1 (1991).
5. Koranne, M., Goodwin, J. G., and Marcelin, G., *J. Catal.* **148**, 388 (1994).
6. (a) Le Bars, J., Auroux, A., Trautmann, S., and Baerns, M., *in* "Proceedings, DGMK Conference Selective Oxidation in Petrochemistry," Ber.-Dtsch. Wiss. Ges. Erdoel, Erdgas Kohle, Tagungsber, p. 59, 1992; (b) Le Bars, J., Auroux, A., Forissier, M., and Vedrine, J. C., *J. Catal.* **162**, 250 (1996).
7. Andersen, P. J., and Kung, H. H., *in* "New Frontiers in Catalysis" (L. Guczi, F. Solymosi, and P. Tetenyi, Eds.), Studies in Surface Science and Catalysis, Vol. 75, p. 205. Elsevier, Amsterdam, 1993.
8. Eon, J. G., Olier, R., and Volta, J. C., *J. Catal.* **145**, 318 (1994).
9. Galli, A., López Nieto, J. M., Dejoz, A., and Vázquez, M. l., *Catal. Lett.* **34**, 51 (1995).
10. Concepción, P., Galli, A., López Nieto, J. M., Dejoz, A., and Vázquez, M. I., *Top. Catal.* **3**, 451 (1996).
11. Blasco, T., Dejoz, A., López Nieto, J. M., and Vázquez, M. l., *J. Catal.* **157**, 271 (1995).
12. Roozeboom, F., Mittelmeljer-Hazeleger, M. C., Moulijn, J. A., Medema, J., de Beer, V. H. J., and Gellings, P. J., *J. Phys. Chem.* **84**, 2783 (1980).
13. Went, G. T., Oyama, S. T., and Bell, A. T., *J. Phys. Chem.* **94**, 4240 (1990).
14. López Nieto, J. M., Kremenic, G., and Fierro, J. L. G., *Appl. Catal.* **61**, 235 (1990).
15. Eckert, H., and Wachs, I. E., *J. Phys. Chem.* **93**, 6796 (1989).
16. Blasco, T., and López Nieto, J. M., *Colloid Surf. A* **115**, 187 (1996).
17. Lapina, O. B., Mastikhin, V. M., Simonova, L. G., and Bulgakova, Yu O., *J. Mol. Catal.* **69**, 61 (1991).
18. Chary, K. V. R., and Kishan, G., *J. Phys. Chem.* **99**, 14424 (1995).
19. Inomata, M., Mori, K., Miyamoto, A., and Murakami, Y., *J. Phys. Chem.* **87**, 761 (1983).
20. Sharma, V. K., Wokaun, A., and Baiker, A., *J. Phys. Chem.* **90**, 2715 (1986).
21. Nag, N. K., and Massoth, F. E., *J. Catal.* **124**, 127 (1990).
22. Kozlowski, R., Pettifer, R. F., and Thomas, J. M., *J. Phys. Chem.* **87**, 5172 (1983).
23. Haber, J., Kozlowska, A., and Kozlowski, R., *J. Catal.* **102**, 52 (1986).
24. Koranne, M., Goodwin, J. G., and Marcelin, G., *J. Catal.* **148**, 369 (1994).
25. Le Bars, J., Vedrine, J. C., Auroux, A., Trautmant, S., and Baerns, M., *Appl. Catal. A* **119**, 341 (1994).
26. Bailes, M., and Stone, F. S., *Catal. Today* **10**, 303 (1991).
27. Kijenski, J., Baiker, A., Glinski, M., Dollenmeier, P., and Wokaun, A., *J. Catal.* **101**, 1 (1986).
28. Akimoto, M., Usami, M., and Echigoya, E., *Bull. Chem. Soc. Japan* **51**, 2195 (1978).
29. Asmolov, G. N., and Krylov, O. V., *React. Kinet. Catal. Lett.* **2**, 11 (1975).
30. Ishida, S., Imamura, S., and Fujimura, Y., *React. Kinet. Catal. Lett.* **43**, 453 (1991).
31. Cavani, F., Centi, G., Trifiró, F., and Grasselli, R. K., *Catal. Today* **3**, 185 (1988).